EurJIC
European Journal of Inorganic Chemistry

Full Papers
doi.org/10.1002/ejic.202001162

Chemistry Europe
European Chemical Societies Publishing

All-alkoxide based deposition and properties of a multilayer $La_{0.67}Sr_{0.33}MnO_3/CoFe_2O_4/La_{0.67}Sr_{0.33}MnO_3$ film

P. Anil Kumar,[a, c] Koroush Lashgari,[b] Sarmad Naim Katea,[b] Olof Karis,[c] Kjell Jansson,[d] D. D. Sarma,[c, e] and Gunnar Westin*[b]

Single and multilayer films of $La_{0.67}Sr_{0.33}MnO_3$ and $CoFe_2O_4$ were deposited by spin-coating. The all-alkoxide precursors allowed inorganic gel films of extreme homogeneity to be formed and converted to phase pure complex oxides at low temperatures. $La_{0.67}Sr_{0.33}MnO_3$ films were made with La- and Ca-methoxyethoxides and $Mn_{19}O_{12}(moe)_{14}(moeH)_{10}$ as precursors at 800 °C. The $CoFe_2O_4$ films were obtained at extremely low 275 °C, using a new $CoFe_2$-methoxyethoxide precursor. The decomposition and microstructural development on heating was described by TG, TEM, XRD and IR spectroscopy. XRD showed no spurious phases and the unit-cell dimensions coincided quite well with literature values of the targeted phases. The structural, magnetic and electronic properties of these films established their phase purity and high quality with physical properties comparable to films deposited by physical deposition methods. The magnetic and magneto transport results are presented for single, bi- and tri- layer structures. The magnetically soft $La_{0.67}Sr_{0.33}MnO_3$ layer was exchange coupled to the magnetically hard $CoFe_2O_4$ layer, giving rise to interesting switching behaviour in magnetism and magneto-transport properties.

Introduction

The interest in transition metal oxides for electronic applications is ever increasing as they are found to exhibit many useful properties, such as magnetoresistance (MR), ferroelectricity, spin-filtering, and metal-insulator transitions.[1,2] Among these, magnetic oxides are seen as potential candidates for developing low energy consuming and faster miniature electronic components, such as memory elements. One of the main criteria for realising successful and viable applications out of the oxide materials is the ease with which these complex compositions can be deposited in the form of thin films[3,4] There has been intense research to meet this challenge leading to the development of various thin film deposition methods, such as molecular beam epitaxy (MBE), pulsed laser deposition (PLD), chemical vapour deposition (CVD) and atomic layer deposition (ALD).[5–8]

Some of these techniques have come a long way in achieving high quality oxide thin films with control over composition and phase purity. However, the physical and chemical vapour based methods are expensive owing to the need of sophisticated equipment. On the other hand, solution-based processing routes provide low cost alternatives to deposit oxide films with complex composition and structure. The success of this approach is critically dependent on the choice of precursors and control of the complex reactions converting the molecular precursors in the solution into the target ceramic film.[9,10] The use of different precursor systems and processing strategies generally lead to very different results. This necessitates detailed studies of the conversion of the molecular precursors into the oxide.[11] Typically, synthesis routes based on highly reactive hetero-metallic single-source alkoxides provide the most elementally homogeneous gels and controllable processes. This arises from the concerted, complete hydrolysis of the different constituent metal alkoxides.[12,13] In contrast, the popular metal organic deposition (MOD) routes using carboxylates and routes using alkoxides mixed with stabilising agents, such as acetylacetonates or carboxylates, typically yield deposits with a large amount of organic residues.[11,14–17] During the heat-treatment, these organic groups cause problems, such as formation of residual carbon, porosity and reduction of metal-ions, such as Fe-, Co-, Ni-, Cu-, Pb-, Bi-ions, resulting in metal particle formation and thereby phase separation. Even if the metal nanoparticles are eventually oxidised by air when the organics have been combusted, a nanoscale phase separation is created that requires heating to higher temperatures to form a homogeneous material. This may cause problems with the substrate and inter-layer atom migration when attempting to form multi-layers. This has hampered the development of high-quality electro-ceramic

[a] Dr. P. A. Kumar
1 Disc Drive, Derry, Northern Ireland, United Kingdom
[b] K. Lashgari, Dr. S. Naim Katea, Prof. G. Westin
Department of Chemistry-Ångström, Ångström Laboratory, Uppsala University, 75121 Uppsala, Schonen Sweden
E-mail: gunnar.westin@kemi.uu.se
[c] Dr. P. A. Kumar, Prof. O. Karis, Prof. D. D. Sarma
Department of Physics and Astronomy, Ångström Laboratory, Uppsala University, 75120 Uppsala, Sweden
[d] Dr. K. Jansson
Department of Materials and Environmental Chemistry, Stockholm University, 10691, Stockholm, Sweden
[e] Prof. D. D. Sarma
Solid State and Structural Chemistry Unit, Indian Institute of Science, Bengaluru 560012, India

Supporting information for this article is available on the WWW under https://doi.org/10.1002/ejic.202001162

films, while the cost and processing efficiency are usually seen as highly competitive, compared to other deposition techniques.

In this work, we investigate the possibility to achieve a high-quality tri-layer structure of two complex oxides, namely the tri-layer stack: $La_{0.67}Sr_{0.33}MnO_3$ (LSMO)/$CoFe_2O_4$ (CFO)/$La_{0.67}Sr_{0.33}MnO_3$ (LSMO), by all-alkoxide based processing. Such films are of great current interest for magnetoresistive and resistive switching devices.[18,19] In addition, this tri-layer structure constitutes a tunnel magnetoresistance junction with a ferrimagnetic barrier (CFO), unlike the usual TMR junctions[18] where the barrier layer is a non-magnetic insulator, typically MgO. Novel effects that may arise in presence of a magnetic tunnel barrier on MR behaviour have been discussed in the literature.[20,21] In the case of a powder composite of LSMO and CFO, it was observed that a strong effect of dipolar coupling led to highly tuneable MR curves.[20] However, in case of a core-shell Fe_3O_4–$CoFe_2O_4$ nanoparticle system, it was observed that the interface exchange coupling, between core and shell materials, dictated the MR behaviour.[21] Such diverse and interesting behaviours make it important to investigate MR structures with magnetic tunnel barriers in the form of multilayers, as is done in the present work.

Herein, we combined an all-alkoxide based sol-gel type process, earlier developed for perovskite films including manganites and cobaltates,[11,13,22] with a new process yielding CFO from a single-source alkoxide. The phase-development from precursor to oxide films of the latter system was investigated. The microstructure and properties of single- and multi-layer oxides were characterised using a wide range of analytical techniques including thermo-gravimetric analysis (TGA), Infrared spectroscopy (IR), X-ray diffraction (XRD), scanning electron microscopy-energy combined with dispersive X-ray spectroscopy (SEM-EDS), transmission electron microscopy (TEM), dc magnetometry and electric transport measurements. Extremely low temperature for CFO synthesis, even without annealing, was found and the properties compared favourably with samples grown by the state-of-the-art physical vapour deposition techniques establishing the viability of solution-based processing for preparing complex oxide hetero-structures.

Results and Discussion

Precursors and conversion of gel to oxide

LSMO: While a number of (oxo)-alkoxides are known for the perovskite A-site ions, including alkali, alkaline earth and rare earth ions, the B-site ions, typically, from the d-block elements, are less accessible, as most are insoluble. Therefore, A-site element alkoxides are usually mixed with B-site element salts, such as acetates, acetylacetonates. As described above, this normally lead to less than optimal films.[9,10] Here, a previously developed all-alkoxide based route yielding high-quality, homogenous LSMO films was used,[11,13] for which the precursor $Mn_{19}O_{12}(moe)_{14}(moeH)_{10}$ was developed.[23]

Metal-alkoxides are very sensitive to water and react instantaneously with moisture in the atmosphere, during spin-coating, to yield inorganic gel films without residual organic groups and solvent. A detailed description of the conversion of an all-alkoxide derived $La_{0.75}Sr_{0.25}Mn$-gel film to LSMO was previously reported.[11] It showed that the gel was converted to a single-phase perovskite through the steps of; (i) loss of water in the temperature range 20–250 °C, and (ii) a multi-step decomposition of carbonate to yield metal-oxide and carbon-dioxide, in the temperature range of 300–600 °C. The carbonate was formed by the absorption of CO_2 from the air by the freshly formed La–Sr–Mn-oxo-hydroxide gel in an acid-base reaction, where the A-site (oxo)-hydroxides are basic and prone to absorption of the acidic carbon dioxide. At the same time, the basic conditions of the fresh gel rendered the Mn^{2+}-ions of the precursor to be easily oxidised into 3+ and 4+ by atmospheric oxygen.

The importance of the thermal profile for the formation of a high quality perovskite thin film was investigated. It was shown that while annealing temperatures, as low as 465 °C, could be sufficient for the perovskite formation, it led to uneven distribution of the A-site ions on a small nanoscale. The reason for this is found in the sequential decomposition of e.g. Ca-, Nd-, and La-carbonates into oxides, respectively. Thus, the various A-site ions are released to react with the Mn-oxide, formed at lower temperatures, at different temperatures. This of course, strongly influences the electric and magnetic properties of the sample.[22] The thermogram of the LSM-gel powder obtained in the present study is shown in Figure 1(a). It matched well with the reaction steps mentioned above and thus, the process is assumed to follow the previous findings. Another interesting fact was that the all-alkoxide derived gels typically had a higher oxidation state of the Mn-ions in the gels than in the corresponding perovskite oxide. This is ascribed to the high basicity of the freshly formed metal-oxo-hydoxo-gels described above. The metastable high oxidation state could be retained in the perovskite where e.g. $La_{0.67}Ca_{0.33}MnO_3$, showed a significant difference in unit cell-dimensions, compared to what is standard in the literature for the composition.[13] This is mainly due to shortened Mn–O bond lengths with the higher Mn-ion charge. However, a short annealing at 800 °C resulted in a loss of the excess oxygen, and a perfect match to the unit-cell reported in the literature.

In view of the above observations, the films in the present study were heated to 850 °C and annealed for 15 min to yield phase pure perovskite of the desired homogeneous A-site ion distribution and oxidation state.

CFO: A single-source molecular precursor, $CoFe_2(O^tBu)_8$ was previously developed for CVD synthesis and thermal decomposition into nanoparticles of $CoFe_2O_4$ at low temperatures.[24] An analogous alkoxide is shown in Figure 2.

Here, the $CoFe_2(O^tBu)_8$ was dissolved in toluene-moeH solvent, which is expected to achieve a ligand exchange between the methoxy-ethoxide (moeH) and O^tBu-groups, yielding methoxy-ethoxide and HO^tBu. It is known that more branched alkoxo-groups are usually exchanged for less branched alkoxo-groups.[26,27] Furthermore, the option of a

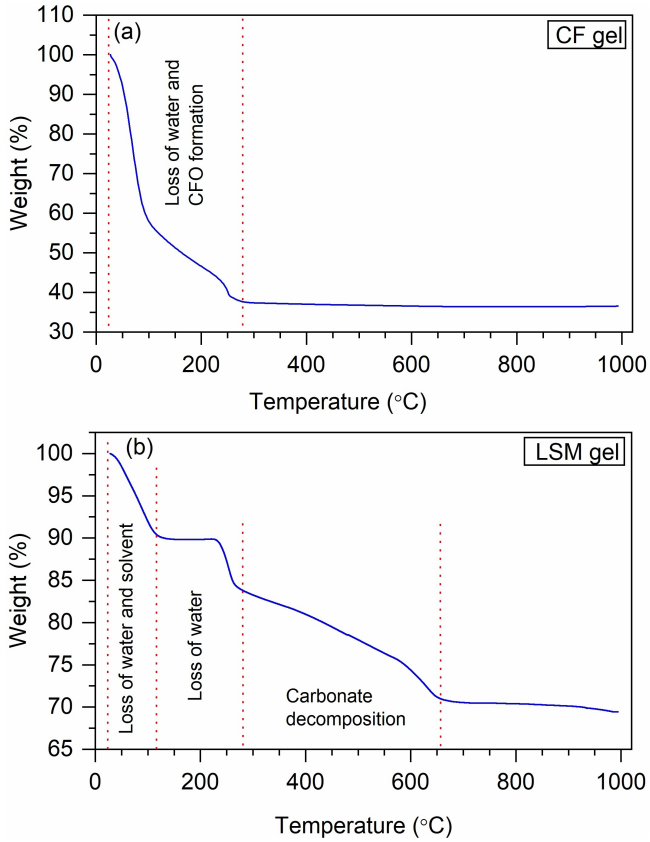

Figure 1. The thermo-gravimetric curves of (a) LSM-gel and (b) CF-gel, respectively, obtained on heating at a rate of 10 °C min^{-1}, in air.

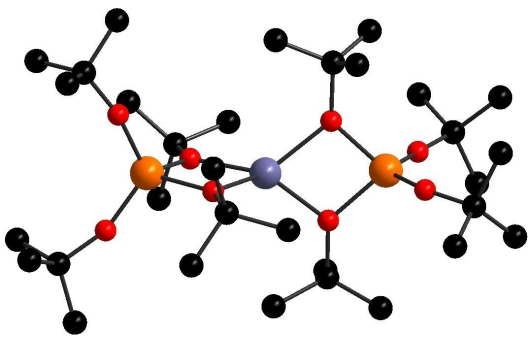

Figure 2. Structure of $CoFe_2(O^tBu)_8$ (Structure data taken from the isostructural $CoAl_2(O^tBu)_8$).[25] In the schematic, the lilac sphere represents Co, the orange spheres represent Fe, the red spheres represent O and the black spheres represent C atoms.

chelating bonding mode, possible with the ether-oxygen of the moe-ligand, should also be a favourable factor, although the moe-ligand often takes a mono-dentate bonding mode.[26,27] However, it is not known if the molecular structure and composition remain after the ligand exchange.

On spin-coating, the CF-alkoxide solution hydrolysed instantaneously to form a gel film. The rather high average acidity of the Co^{2+}- and two Fe^{3+}-ions makes it less likely to form stable metal carbonates, as was observed for the LSM-gel. The reaction steps involved in the formation of the $CoFe_2O_4$ phase were determined by thermo-gravimetric analysis of the $CoFe_2$-gel powder. As seen in Figure 1(b), heating of the gel, in air at 10 °C min^{-1}, resulted in a large weight-loss up to 100 °C, ascribed as due to loss of loosely bonded water and solvent. Further heating resulted in a rather continuous weight-loss until 240 °C. Subsequently, a rapid weight-loss took place, ending at 275 °C, and was followed by a close to constant weight to 1000 °C. The mass at 240 °C roughly corresponded to a composition of $CoFe_2O_2(OH)_4$, assuming the product at 300 °C to be $CoFe_2O_4$.

The XRD derived unit cell-parameter, using the cubic spinel (Fd3 m) system, was determined to be a = 8.363 Å. This corresponds quite well to literature values and indicates that the CFO was of the proper composition.[28]

The TEM image, given in Figure 3(a), shows that the CF-gel was amorphous with only a few places showing barely discernible atomic ordering in domains of less than 1 nm. Such emerging crystallisation may be the result of heating by the electron beam in the high vacuum, knowing that only 275 °C is required, at atmosphere pressure, to release the water and yield CFO. The EDS point analyses showed that the material was homogeneous with the ~20 nm probe size.

The TEM image given in Figure 3(b and c) of the gel heated to 300 °C, shows the formation of evenly sized crystallites of $CoFe_2O_4$ with a diameter of 3–5 nm (average 3.4 nm) throughout the material. Actually, annealing for 30 min, at as low temperature as 250 °C could be used to obtain CFO. The broad XRD peaks obtained fitted a CFO unit cell-parameter of a = 8.354 Å and a crystallite size of 1.4 nm, as given in the supporting information, Figure S1.

Thus, the homogenous crystallisation of CFO particles occurred at a very low temperature of below 300 °C. This indicates an extremely high, most probably atomic scale mixing, of the constituent ions in the gel, requiring only a small thermal energy to condense the –OH groups to release H_2O. Hence, no substantial migration of metal-ions would be needed. Furthermore, heating of the films resulted in the growth of CFO crystallites.

$La_{0.67}Sr_{0.3}MnO_3/CoFe_2O_4$ multi-layer films. Single- and multi-layer films were prepared on Al_2O_3 (0001) substrate by spin-coating LSM- or CF-alkoxide solutions in air at 3900 rpm. The gel films thereby obtained were heated to 850 °C at 10 °C min^{-1}, in a tube furnace with ambient atmosphere, followed by annealing at the temperature for 15 minutes and cooling to room temperature.

The mono-, bi- or tri- layers of the LSMO/CFO films were prepared by spin-coating the solutions of the next layer followed by an identical heat-treatment in the desired sequence. Single LSMO and CFO layer films were also prepared for comparison.

Figure 4 presents the grazing incidence XRD patterns of tri-layer films. Diffraction peaks corresponding to LSMO and CFO phases were observed, as given with their corresponding indices (hkl). No impurity peaks were found. The unit cell-parameters for the CFO and LSMO phases in the tri-layer LSMO/CFO/LSMO film were determined with the Bruker AXS Topas software. The CFO phase had a cubic (Fd-3m) unit-cell

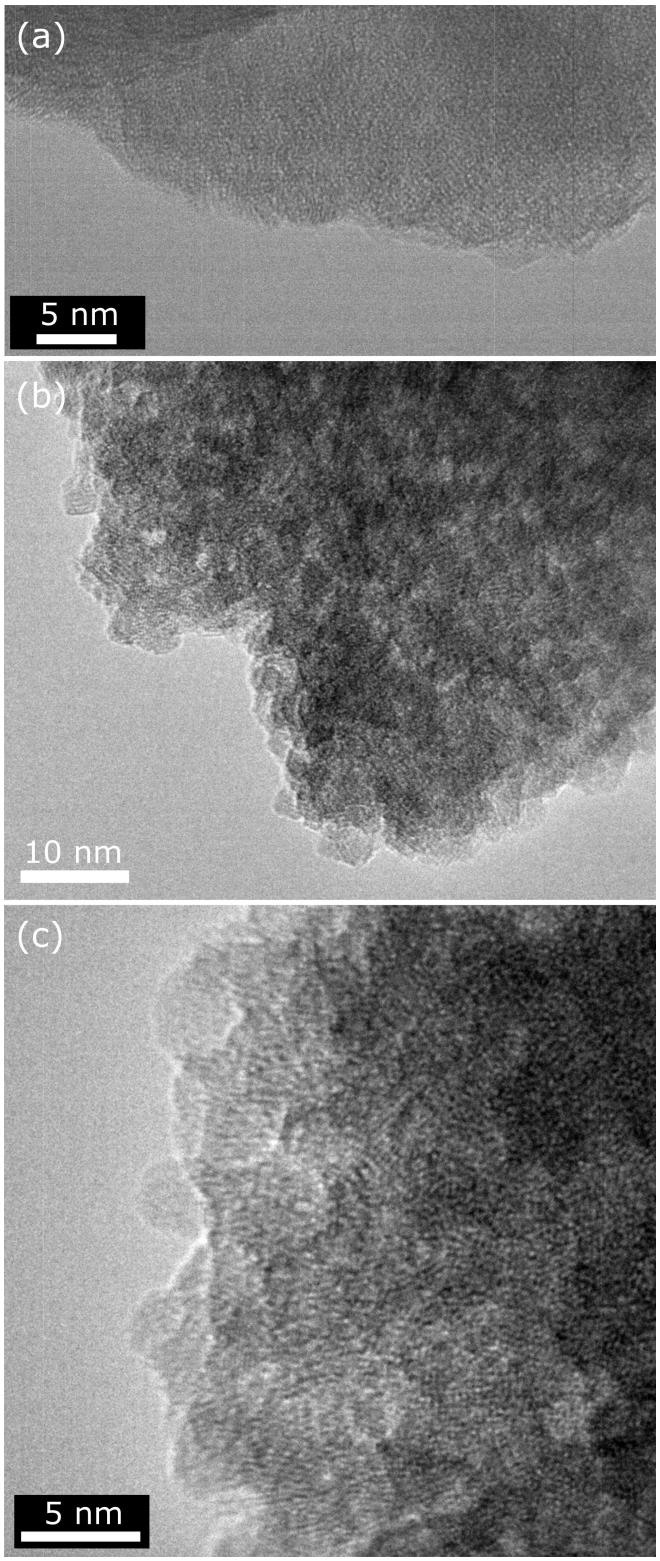

Figure 3. The TEM images of (a) CF-gel and (b and c) of the product $CoFe_2O_4$ obtained after heating the CF-gel to 300 °C, given at different enlargements.

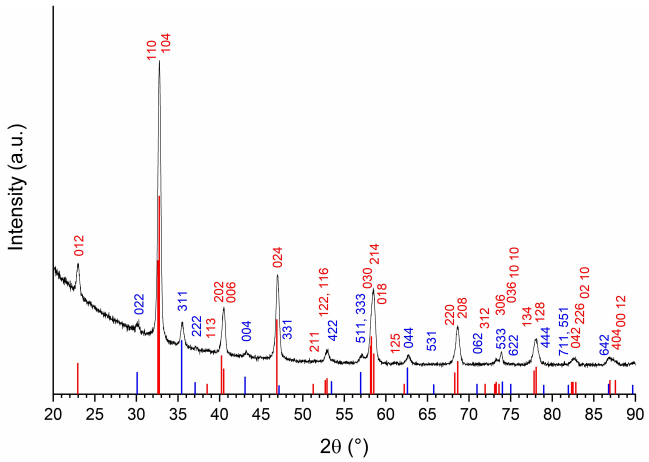

Figure 4. GI-XRD patterns of the LSMO/CFO/LSMO film on Al_2O_3 (0001) substrate. The red and blue bars, and hkl identifiers mark the LSMO and CFO phases, respectively.

parameter of a = 8.379(1) Å, which fits the literature value of a = 8.39190 Å, within 0.15 %.[28] The LSMO phase was determined using an orthorhombic (R-3c:H) unit-cell with a = 5.4788(6) Å and c = 13.357(2) Å. This fits the literature values of a = 5.4900 Å and c = 13.3560 Å, within 0.4 % for the $La_{0.67}Sr_{0.33}MnO_3$ composition.[29] The first LSMO layer gave the unit-cell dimensions a = 5.495 Å and c = 13.360 Å, thus also fitting the literature values quite well.

This shows that the CFO and LSMO phases were pure and of the proper composition, even after the multi-layer deposition. Reliable crystallite size determination from the XRD peak broadening is hard get, due to the complex shape of the crystallites, but the obtained sizes around of ~25–35 nm, corresponded well with the grain sizes observed in the TEM images. The relative peak intensities and XRD peak data indicated that the films were polycrystalline without significant epitaxial preferences. An SEM image of the LSMO film surface is shown in Figure 5(a), which further corroborates the polycrystalline nature of the films. The SEM image also showed that the films consisted of interconnected grains, with pinholes, a few nanometres in size, in the grain boundaries. An image analysis indicated that the pores constituted roughly 7 % of the area. The cross-sectional TEM image, shown in Figure 5(b), of the tri-layer [Al_2O_3]/LSMO/CFO/LSMO film, clearly shows that the film consists of LSMO and CFO granular layers of ~35 nm and ~25 nm average thickness, respectively and that there was no sign of reaction/inter-diffusion between the layers.

Electronic and magnetic properties. Electronic and magnetic properties of oxide materials are often sensitive to variations in their chemical compositions, as well as the homogeneity of the samples. Therefore, the electronic and magnetic properties of the present films were studied to understand the quality of the films produced by the all-alkoxide sol-gel method employed here. Figure 6 presents the field-cooled magnetisation versus temperature curves, M–T, of the bi-layer ([Al_2O_3]/CFO/LSMO) and tri-layer ([Al_2O_3]/LSMO/CFO/LSMO) films, along with the LSMO film for comparison. The measurements were carried out under a magnetic field of 20 Oe. The LSMO control film showed a sharp ferromagnetic transition with a Curie temperature (T_C) of about 350 K. This

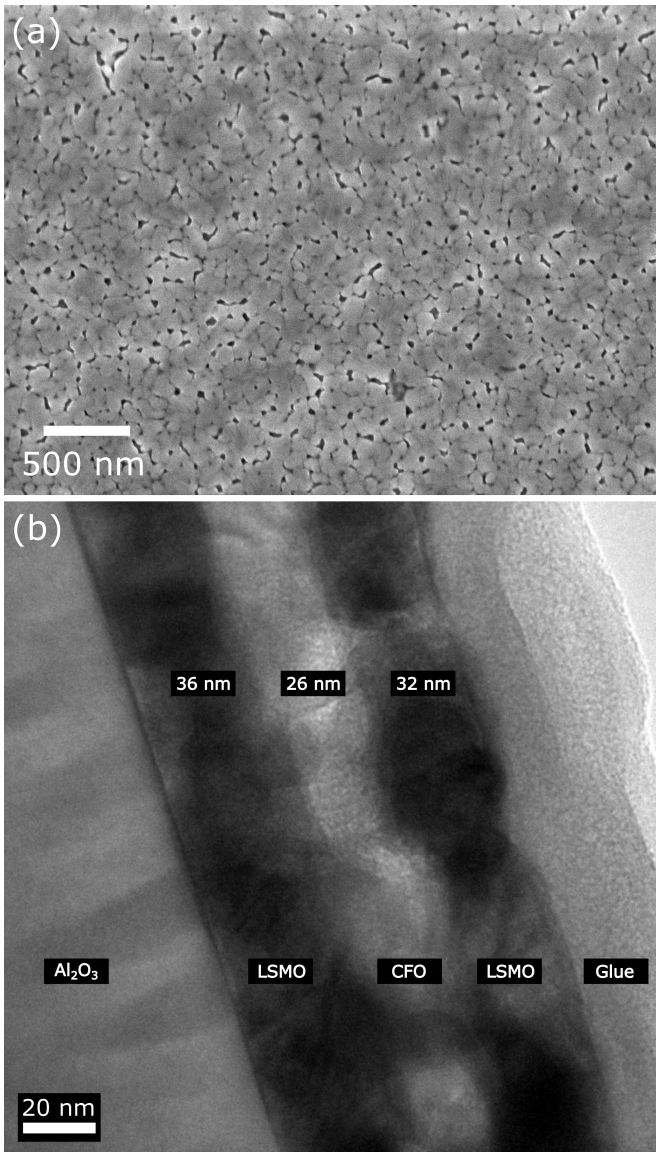

Figure 5. Panel (a) shows the SEM image of the top LSMO layer for the film LSMO/CFO/LSMO and panel (b) shows the cross-sectional TEM image of the LSMO/CFO/LSMO film.

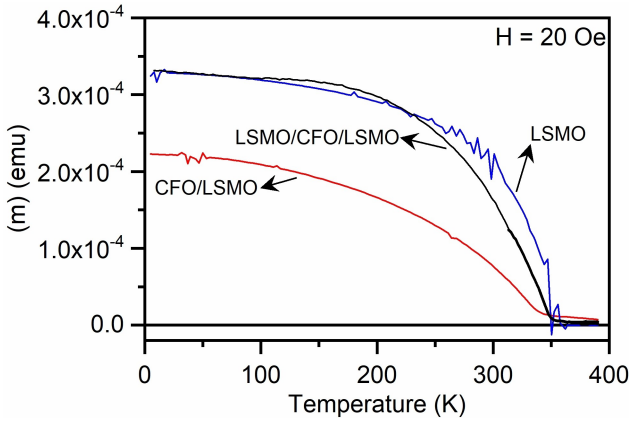

Figure 6. Temperature dependence of magnetic moment for the single $[Al_2O_3]$/LSMO layer, $[Al_2O_3]$/CFO/LSMO bi-layer, and $[Al_2O_3]$/LSMO/CFO/LSMO tri-layer, measured on cooling from 390 K under a field of 20 Oe.

value is close to the T_C value of ~380 K, reported for bulk LSMO with an identical composition.[30]

The agreement between the critical temperatures of LSMO films prepared by the all-alkoxide route used in our studies with those reported for bulk LSMO indicates that the films are of high compositional quality and homogeneity. Since the magnetic transition temperature depends on the composition, the homogeneity and the phase purity are also indicated by the smooth variation of the M–T plot without any evidence for the presence of any secondary magnetic transition anywhere. The all-alkoxide solution deposition reported here is comparable to the films prepared by other physical techniques, such as pulsed laser deposition[31] and sputtering[32] which produce LSMO films with T_C values of ~340 K and ~347 K, respectively. Markedly, the present all-alkoxide method produces films with higher T_C, compared to conventional sol-gel methods using metal salts as precursors.[14–17,33] The bi- and tri-layer films also showed a ferromagnetic transition around 350 K, as clearly observed for the control LSMO film. The finite magnetisation observed in the bi- and tri- layer films above 350 K was due to the ferrimagnetic contribution from CFO whose bulk transition temperature is ~825 K.[34]

Isothermal magnetic moment versus magnetic field curves (hysteresis loops) for $[Al_2O_3]$/LSMO and $[Al_2O_3]$/CFO films, measured at 5 K, are presented in Figure 7(a) and (b), respectively. The control LSMO film exhibited a magnetic coercivity of ~390 Oe. Furthermore, the LSMO layer showed a high remanence due to an in-plane anisotropy. In contrast, the magnetic coercivity of the CFO film, ~12 kOe, was high, but this is largely attributable to high magneto-crystalline anisotropy of CFO.[35] The hysteresis loops of the $[Al_2O_3]$/CFO/LSMO and $[Al_2O_3]$/LSMO/CFO/LSMO composite films are presented in Figure 7(c) and (d), respectively. The composite films exhibited two magnetic switching fields, corresponding to the coercive fields of both LSMO and CFO. For example, in the $[Al_2O_3]$/LSMO/CFO/LSMO sample, the LSMO layers switched their magnetisation at ~360 Oe, whereas the CFO magnetisation switching occurred at ~10 kOe.

Along with the magnetic behaviour, the electronic transport, especially the magnetoresistance properties of the manganites are suitable indications to the quality of the present films. The electrical resistance of the LSMO film and the tri-layer film, LSMO/CFO/LSMO, as a function of temperature, are shown in Figure 8(a) and (b), respectively. The resistances of these films (both LSMO and the tri-layer thin films) were measured in current-in-plane (CIP) configuration with four silver electrodes painted on the top of the LSMO film. The LSMO film showed a broad transition at T ~225 K, which is characteristic of a metal-insulator (MI) transition. It is generally observed that in this class of manganites, the metal-insulator transition and the ferromagnetic-paramagnetic transition are interrelated and occur at close temperatures.[36]

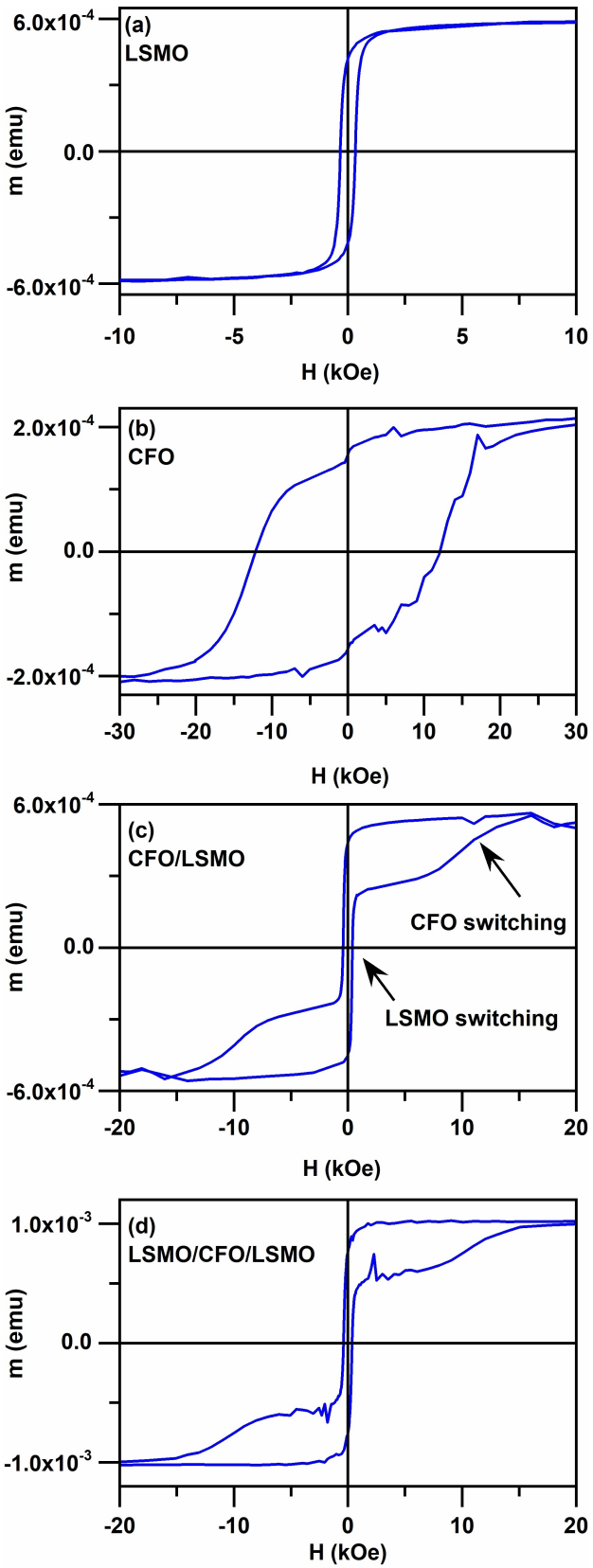

Figure 7. The M versus H data measured at 5 K for the films (a) [Al_2O_3]/LSMO, (b) [Al_2O_3]/CFO, (c) [Al_2O_3]/CFO/LSMO and (d) [Al_2O_3]/LSMO/CFO/LSMO.

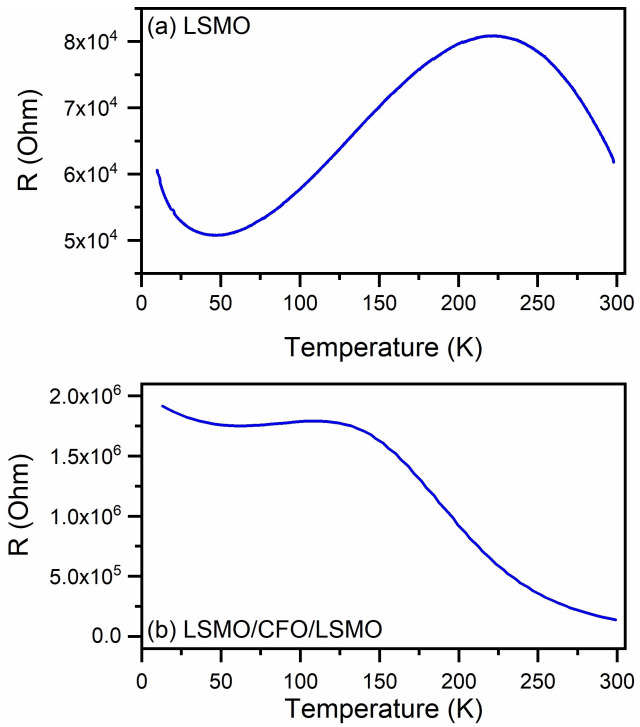

Figure 8. Temperature variation of resistance of films (a) LSMO and (b) LSMO/CFO/LSMO deposited on Al_2O_3 (0001). The data corresponds to current-in-plane geometry.

However, in the present LSMO film, the MI transition temperature was much lower than that of the ferromagnetic transition. This deviation is possibly a result of an extrinsic influence on the resistivity based on the granular character of the film.[37] It is known that both magnetic and metal-insulator transitions in LSMO depend critically on the Sr and oxygen compositions with a decrease in either of the two leading to a suppression of the transition temperatures; so it is possible that the grain boundary regions are slightly less doped and therefore, with a lower transition temperature. This would limit the transport properties in a dominant manner in such a granular film with grain boundaries separating the grains, while the magnetic properties will be much less affected arising from the grain surface constituting a small volume fraction of the film. The LSMO film also exhibited a low temperature upturn in the resistance curve below 50 K. A similar behaviour has been reported elsewhere, where it was attributed to electron-electron interactions.[38]

Alternatively, the upturn may be a result of disorder in the grain boundaries. In the tri-layer LSMO/CFO/LSMO, the presence of the insulating CFO layer significantly altered resistance versus temperature curve. In addition, in the tri-layer film, the resistance value was about an order of magnitude higher than that in the LSMO film, evidently due to the presence of the highly insulating CFO layer sandwiched between top and bottom LSMO layers.

The class of perovskite manganites to which LSMO belongs is investigated intensely for their magnetoresistance properties

owing to the high spin-polarisation in these materials. Therefore, the magnetoresistance behaviours of the present films were investigated to determine the quality of the films and to study the effects of $CoFe_2O_4$ proximity on the MR behaviour of LSMO. Figure 9 shows the MR% variation with magnetic field for the LSMO film. The MR% is defined as, $100\times(R(H)-R_{peak})/R_{peak}$), where R_{peak} is the peak resistance (R) of the film as a function of the applied magnetic field (H) at a fixed temperature. The data obtained for different sample temperatures is shown in the Figure 9, as indicated. The magnetoresistance behaviour of the granular LSMO film is characteristic of tunneling type magnetoresistance, where reduction in the resistance is observed due to the magnetic field induced magnetic alignment of the neighbouring grains. It was also observed that at lower temperatures, there was an increase in the magnitude of the MR%. This increase in MR was due to the increase in the degree of magnetic alignment with decreasing temperature. The magnitude of MR% (~22% at 9.5 K and 3.5 kOe) is comparable to what is usually reported for LSMO. This also confirms the quality of the films prepared by the all-alkoxide based sol-gel technique. The peak in the MR curve occurred at a value H_C^{MR}, which is slightly higher than the magnetic coercivity, H_C, of the LSMO film. For example, the value of H_C at 5 K was ~390 Oe (from Figure 7(a)) but the value of H_C^{MR}, at the closest temperature, 9.5 K was ~450 Oe. The higher value of H_C^{MR}, compared to magnetic coercivity, may indicate that the insulating grain boundary had a higher magnetic coercivity than that of LSMO. In addition, it is depicted in the inset of Figure 9, that the value of H_C^{MR} increased with a decreasing temperature. The observation is in accordance with the fact that the magnetic coercivity of a ferromagnetic sample increases with a decrease in the temperature.

Results of magnetotransport measurements on the tri-layer LSMO/CFO/LSMO film are presented in Figure 10. In these plots, the MR% of the tri-layer sample is plotted as a function of applied magnetic field at 10 K. The data in Figure 10(a) were measured with the zero-field-cooled (ZFC) and field-cooled (FC)

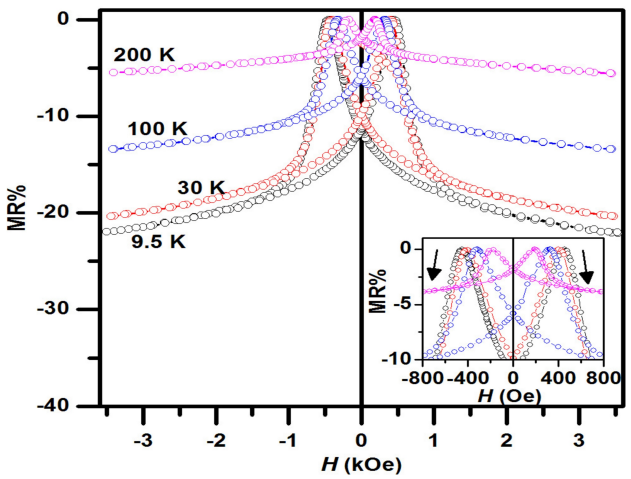

Figure 9. The magneto-resistance (MR%) versus magnetic field data for the LSMO film at different temperatures. The inset shows the low field data to highlight the change in peak positions as a function of temperature.

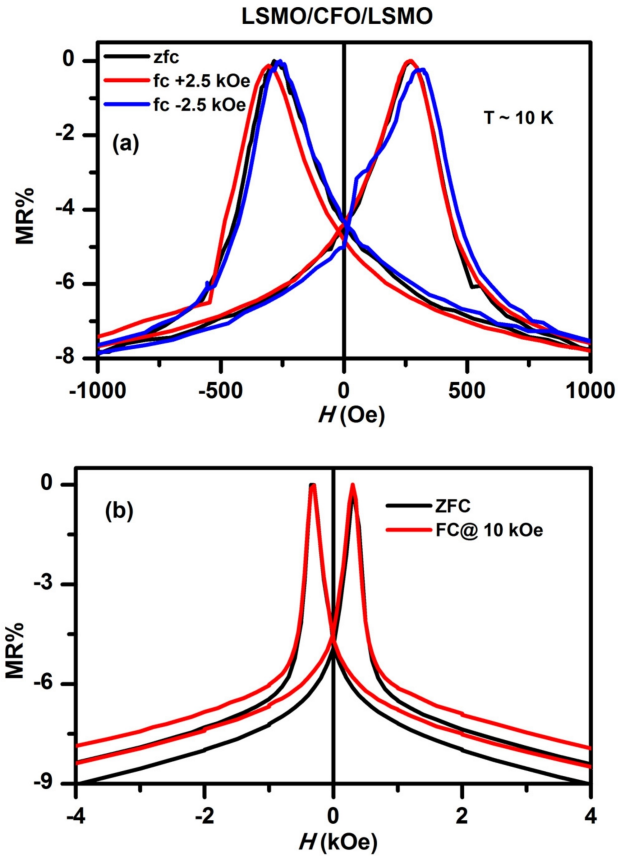

Figure 10. The magneto-resistance data for the trilayer film LSMO/CFO/LSMO is presented. Panel (a) shows the data measured up to a maximum field of ±3.5 kOe for zero-field-cooled (ZFC) and two different field-cooled (FC) conditions as indicated in the legend. The data in panel (b) corresponds to the measurement up to a maximum field of ±70 kOe and in ZFC and FC (with 10 kOe cooling field) configurations.

configurations with two different cooling fields of +2.5 kOe or −2.5 kOe, and up to a measurement field of about ±3.5 kOe. In the ZFC curve, characteristic peaks are observed at magnetic fields which are close to the magnetic coercivity values of the LSMO film. Since the resistance was measured in CIP configuration, and the magnetic state of LSMO almost completely determines the resistance of the film, it is natural that the highest resistance in the ZFC curves occurred near the magnetic coercivity value of LSMO. However, an interlayer exchange coupling seems to exist between the LSMO and the CFO layers, as explained below. This exchange coupling between LSMO and CFO, in combination with the higher magnetic coercivity of CFO, influences the magnetic state of LSMO layer in FC condition. This is evident from the observation that the ZFC and FC curves are relatively shifted in field axis, which signifies an exchange coupling between the magnetically soft LSMO and hard CFO layers.

Additionally, the sign of cooling field, representing the direction of the applied magnetic field during the cooling of the sample, also affected the MR curves. A positive field cooling resulted in a negative shift whereas the negative field cooling resulted in a positive shift of the MR curves. This shifting of the

MR curves to the opposite sense with respect to their cooling fields arises from the fact that the CFO layer moment is locked in the direction of cooling field and, in its turn, also locks with it the LSMO layer moment. Thus, a higher magnetic field was needed to magnetize the LSMO layer in the direction opposite to the cooling field direction. In contrast, the FC resistance measurements carried out to higher magnetic fields did not show any such difference when compared to ZFC measurement. This is shown in Figure 10(b), where the cooling field is 10 kOe and the measurement was carried out until $\pm$70 kOe. When the measuring magnetic field was limited to 3.5 kOe (smaller than the coercivity of the CFO layer), the shifting of resistance-field curves was due to an interfacial exchange bias between the LSMO and CFO layers. However, in the latter set of measurements, where the measuring field (70 kOe) was sufficient to flip the magnetic moment of the underlying CFO layer, no such shift in resistance-field curve was observed.

Conclusions

Multilayer LSMO/CFO films have been deposited using all-alkoxide solution-based routes optimised to attain best quality films. A new route to CFO films using $CoFe_2(O^tBu)_8$ as precursor was developed and its phase development on heating investigated. It was found that pure CFO formed at as low a temperature as 275 °C, which is ascribed to the extreme elemental homogeneity and compositional precision in the precursor. This film was successfully combined with an earlier developed all-alkoxide process for $La_{0.70}Sr_{0.30}MnO_3$ films to achieve multi-layer structures of these two compositions.

The measured magnetic properties were comparable to what is expected for high quality films of the same composition prepared by state-of-the-art vacuum-based techniques. The transport properties were influenced by the presence of grain boundaries and pinholes in the film. It is likely possible to optimise the thermal processing further to achieve very high densities of the films that will improve the transport properties. However, from the present work, it can be seen that all-alkoxide processing, which is considered cheaper and more efficient than PVD and CVD, have a great potential for preparing complex oxide super-lattice structures.

The LSMO film showed a broad transition at T ~ 225 K, which is characteristic of a metal-insulator (MI) transition. It is generally observed that in this class of manganites, the metal-insulator transition and the ferromagnetic-paramagnetic transition are interrelated and occur at close temperatures.[36]

Experimental Section

Chemicals and Equipment. All synthesis and manipulations of the precursor solutions were made in a glove-box) with dry, oxygen free Argon (MBraun, < 1ppm O_2, H_2O. The Sr metal (dendritic from Sigma-Aldrich with a purity of 99.9%), La metal (chips from Sigma-Aldrich with 99.9% purity) and $MnCl_2$ (anhydrous from Sigma-Aldrich with a purity of 99.99%) were used as received, while the solvents, methoxy-ethanol (moeH) and toluene were dried by distillation over CaH_2 before use. The commercially purchased Al_2O_3 (0001) substrates were cleaned in running de-ionized water followed by rinsing in acetone and drying immediately.

Preparation of all-alkoxide precursors. The LSMO solution was prepared in a way closely following what has been reported for other manganites, including $La_{0.75}Sr_{0.25}MnO_3$. Here, Sr(II)-methoxy-ethoxide (Sr-moe), La(III)-methoxy-ethoxide (La-moe), were synthesised by dissolving the metals in moeH : toluene solution under evolution of hydrogen, as described elsewhere.[11,13] The concentration was determined by gravimetric analysis, after a heat-treatment of a precisely known volume of metal-alkoxide at 1050 °C for 18 h, or through complexometric titration with EDTA. The Mn(II)-oxo-methoxy-ethoxide, determined by single crystal X-ray diffraction, to have the molecular composition $Mn_{19}O_{12}(moe)_{14}(moeH)_{10}$, (Mn-moe) was prepared by metathesis of $MnCl_2$ and 2 Kmoe in moeH : toluene solvent, as described elsewhere.[23] The concentration of the pink solution obtained was determined gravimetrically as Mn_3O_4, after heat-treatment at 1000 °C for 4 hours in air.

The LSMO precursor solution was prepared by mixing appropriate amounts of the La-moe, Sr-moe and Mn-moe solutions and moeH : toluene solution to yield a ca. 0.5 M (metal) solution with the composition La : Sr:Mn (2 : 1 : 3). The single-source $CoFe_2(O^tBu)_8$ precursor, was obtained from the laboratory of Prof. Sanjay Mathur, University of Cologne, Germany, as a sublimed powder.[24] An analogous structure is shown in Figure 2. The $CoFe_2(O^tBu)_8$ powder was dissolved in toluene : moeH to yield a solution with a total metal concentration of 0.33 M. This solution was filtered through a 20 nm Anotop alumina membrane (from Whatman) to remove suspended particles and get a clear dark coloured solution. It is expected from the literature that the O^tBu ligands are replaced by moe ligands in this process. Therefore, the precursor is given as $CoFe_2$-moe.

Analytical techniques. For studies of the gel and phase-development on heating, the $CoFe_2$-moe and the La-, Sr-, Mn-moe solutions were deposited on a Petri-dish, in air. Both solutions reacted instantaneously to form solids that easily turned into powders when the solvent had evaporated after a few minutes. The perovskite forming solution and phase development on heating has been described in detail elsewhere,[11] and was therefore studied only on key parameters here. The spinel forming solution and gel-to-oxide conversion was described in more detail. The thermal decomposition the air-hydrolysed deposit was studied by thermo-gravimetric analysis (TGA) in air, using a Netsch-STA409 apparatus. A heating rate of 10 °C min^{-1} was used. The gels and samples obtained by heating to temperatures of interest were studied with a combination of techniques: X-ray diffraction (XRD), using a D5000 diffractometer in θ–2θ mode from Siemens, using Cu Kα radiation, and a transmission electron microscopy (TEM) using a Jeol 2100F instrument, operating at 200 kV, and equipped with an energy dispersive spectrometer (EDS). CFO films were investigated after scraping off powder from a film deposited and heated on a Si/SiO_2 substrate.

The tri-layer LSMO/CFO/LSMO film on α-Al_2O_3 substrate was studied on its microstructure with a FEI Technai TEM on suitably prepared cross-sections, while the surfaces of di- and tri-layers were studied with a JEOL field emission type scanning electron microscope (SEM). Grazing incidence x-ray diffraction (GI-XRD) was obtained with a Siemens D5000 instrument. The unit-cell- dimensions of films and powders were obtained with the Bruker AXS Topas 4.2 software, using the peaks in the range 20–90° 2θ. A standard α-Al_2O_3 substrate was used to get instrument parameters.

The magnetic measurements were performed using a Quantum Design MPMS-XL SQUID magnetometer and the magnetic field, temperature dependence of resistance was measured using a home-built resistance setup with a four-probe configuration.

Acknowledgements

The authors thank S. C. Purandare and Pushan Ayyub from TIFR, India for their support with TEM investigations. The authors also thank Swedish Foundation for International Cooperation in Research and Higher Education (STINT) and the Swedish Research Council (grants: 2016-04524) for supporting this research. DDS thanks Science and Engineering Research Board and Department of Science and Technology, Government of India and Jamsetji Tata Trust for support of this research. This work was performed, in part, at the Electron Microscopy Centre, supported by the Department of Materials and Environmental Chemistry and Faculty of Science at Stockholm University.

Conflict of Interest

The authors declare no conflict of interest.

Keywords: multi-layer film · sol-gel · alkoxide · CFO · LSMO

[1] M. Bibes, J. E. Villegas, A. Barthélémy, *Adv. Phys.* **2011**, *60*, 5–84.
[2] Z. Yang, C. Ko, S. Ramanathan, *Ann. Rev. Mater. Res.* **2011**, *41*, 337–367.
[3] L. W. Martin, Y.-H. Chu, R. Ramesh, *Mater. Sci. Eng. R* **2010**, *68*, 89–133.
[4] R. W. Johnson, A. Hultqvist, S. F. Bent, *Mater. Today* **2014**, *17*, 236–246.
[5] A. L. Kobrinskii, *Epitaxial Perovskite Magnetic Oxide Thin Films and Bilayers*; University of Minnesota, **2007**.
[6] M. Bibes, A. Barthélémy, *IEEE Trans. Electron Devices* **2007**, *54*, 1003–1023.
[7] M. R. Catalano, G. Cucinotta, E. Schilirò, M. Mannini, A. Caneschi, R. Lo Nigro, E. Smecca, G. G. Condorelli, G. Malandrino, *Chem. Open* **2015**, *4*, 523–532.
[8] O. Nilsen, E. Rauwel, H. Fjellvåg, A. Kjekshus, *J. Mater. Chem.* **2007**, *17*, 1466–1475.
[9] C. D. Chandler, C. Roger, M. J. Hampden-Smith, *Chem. Rev.* **1993**, *93*, 1205–1241.
[10] R. W. Schwartz, *Chem. Mater.* **1997**, *9*, 2325–2340.
[11] G. Westin, A. Pohl, M. Ottosson, K. Lashgari, K. Jansson, *J. Sol-Gel Sci. Technol.* **2008**, *48*, 194–202.
[12] D. Iuşan, R. Knut, B. Sanyal, O. Karis, O. Eriksson, V. A. Coleman, G. Westin, J. M. Wikberg, P. Svedlindh, *Phys. Rev. B* **2008**, *78*, 085319.
[13] A. Pohl, G. Westin, K. Jansson, *Chem. Mater.* **2002**, *14*, 1981–1988.
[14] A. Haque, A. R. Mahbub, A.-A. Mamun, M. Reaz, K. Gosh, *Appl. Phys. A* **2019**, *125*, 357, 1–9.
[15] X. Tang, R. Wei, L. Hu, X. Zhu, J. Yang, J. Dai, W. Song, X. Zhu, Y. Sun, *J. Appl. Phys.* **2017**, *121*, 245305, 1–6.
[16] X. Tang, X. Zhu, R. Wei, L. Hu, J. Yang, W. Song, J. Dai, X. Zhu, Y. Sun, *Composites Part B* **2020**, *186*, 107801, 1–7.
[17] P. Richter, P. N. Plassmeyer, J. Harzdorf, T. Ruffer, H. Lang, J. Kalbacova, N. Jöhrmann, S. Schultze, M. Hietschold, S. S. P. K. Arekapudi, M. Albrecht, D. R. T. Zahn, C. J. Page, G. Salvan, *Chem. Mater.* **2016**, *28*, 4917–4927.
[18] D. D. Sarma, S. Ray, K. Tanaka, M. Kobayashi, A. Fujimori, P. Sanyal, H. Krishnamurthy, C. Dasgupta, *Phys. Rev. Lett.* **2007**, *98*, 157205.
[19] V. Thakare, G. Xing, H. Peng, A. Rana, O. Game, P. A. Kumar, A. Banpurkar, Y. Kolekar, K. Ghosh, T. Wu, D. D. Sarma, S. B. Ogale, *Appl. Phys. Lett.* **2012**, *100*, 172412.
[20] P. A. Kumar, D. D. Sarma, *Appl. Phys. Lett.* **2012**, *100*, 262407.
[21] P. A. Kumar, S. Ray, S. Chakraverty, D. D. Sarma, *Appl. Phys. Lett.* **2013**, *103*, 102406.
[22] A. Pohl, G. Westin, *J. Mater. Res.* **2011**, *22*, 1737–1743.
[23] I. A. Pohl, L. G. Westin, M. Kritikos, *Chem. Eur. J.* **2001**, *7*, 3438–3445.
[24] S. Mathur, C. Cavelius, K. Moh, H. Shen, J. Bauer, *Z. Anorg. Allg. Chem.* **2009**, *635*, 898–902.
[25] F. Meyer, R. Hempelmann, S. Mathur, M. Veith, *J. Mater. Chem.* **1999**, *9*, 1755–1763.
[26] D. C. Bradley, R. C. Mehrotra, I. P. Rothwell, A. Singh, *Alkoxo and Aryloxo Derivatives of Metals*; Elsevier, **2001**.
[27] K. G. Caulton, L. G. Hubert-Pfalzgraf, *Chem. Rev.* **1990**, *90*, 969–995.
[28] PDF file: 00-022-1086 Natl. Bur. Stand. (U. S.) *Monogr. 25.* **1971**, *9*, 22.
[29] PDF-file: 00-050-0308, V. Zubkov, Inst. Solid State Chem., Ekaterinburg, Russia, **1998**.
[30] H. Hwang, S. Cheong, N. Ong, B. Batlogg, *Phys. Rev. Lett.* **1996**, *77*, 2041–2044.
[31] Y. Takamura, R. V. Chopdekar, E. Arenholz, Y. Suzuki, *Appl. Phys. Lett.* **2008**, *92*, 162504.
[32] P. Dey, T. K. Nath, A. Taraphder, *Appl. Phys. Lett.* **2007**, *91*, 012511.
[33] M. Zarbali, A. Göktaş, I. H. Mutlu, S. Kazan, A. G. Şale, F. Mikailzade, *J. Supercond. Novel Magn.* **2011**, *25*, 2767–2770.
[34] J. A. Paulsen, C. C. H. Lo, J. E. Snyder, A. P. Ring, L. L. Jones, D. C. Jiles, *IEEE Trans. Magn.* **2003**, *39*, 3316–3318.
[35] C. N. Chinnasamy, B. Jeyadevan, K. Shinoda, K. Tohji, D. J. Djayaprawira, M. Takahashi, R. J. Joseyphus, A. Narayanasamy, *Appl. Phys. Lett.* **2003**, *83*, 2862–2864.
[36] Y. Tokura, Y. Tomioka, *J. Magn. Magn. Mater.* **1999**, *200*, 1–23.
[37] R. D. Sánchez, J. Rivas, C. Vázquez-Vázquez, A. López-Quintela, M. T. Causa, M. Tovar, S. Oseroff, *Appl. Phys. Lett.* **1996**, *68*, 134–136.
[38] A. Chainani, M. Mathew, D. D. Sarma, I. Das, E. V. Sampathkumaran, *Physica B +C* **1993**, *186–188(C)*, 995–997.
[39] C. J. Adkins, *J. Phys. Condens. Matter.* **1989**, *1*, 1253–1259.

Manuscript received: December 25, 2020
Revised manuscript received: February 22, 2021
Accepted manuscript online: March 1, 2021